Journal of Inorganic Biochemistry 197 (2019) 110690

Contents lists available at ScienceDirect

Journal of Inorganic Biochemistry

journal homepage: www.elsevier.com/locate/jinorgbio

Rapid sequential detection of Hg^{2+} and biothiols by a probe DNA—MOF hybrid sensory system

Nai-Han Huang[1], Rong-Tian Li[1], Cheng Fan, Ke-Yang Wu, Zhe Zhang, Jin-Xiang Chen*

Guangdong Provincial Key Laboratory of New Drug Screening, Guangzhou Key Laboratory of Drug Research for Emerging Virus Prevention and Treatment, School of Pharmaceutical Sciences, Southern Medical University, Guangzhou 510515, PR China

ARTICLE INFO

Keywords:
Metal–organic framework
Hg^{2+} sensing
Biothiols sensing
Sequential fluorescence detection

ABSTRACT

A one-dimensional (1D) metal–organic framework (MOF) of $[Cu(Cdcbp)(H_2O)_2{\cdot}2H_2O]_n$ (**1**, H_3CdcbpBr = 3-carboxyl-(3,5-dicarboxybenzyl)-pyridinium bromide) has been synthesized and characterized. MOF **1** features a cationic Cu^{2+} center, conjugated tricarboxylate ligand bearing positively charged pyridinium and uncoordinated carboxylate groups within its skeleton. These features enable MOF **1** to tightly adsorb thymine rich (T-rich) single-stranded DNA (ss-DNA) probe labeled with carboxyfluorescein (FAM) (denote as P-DNA) through π-stacking, electrostatic interactions and/or hydrogen bonding to give a hybrid complex (denote as P-DNA@**1**), and quenches its fluorescence via a photo-induced electron transfer (PET) process. The formed P-DNA@**1** hybrid can thus function as a sensing platform for the detection of Hg^{2+}, driven by the formation of hairpin-like double-stranded DNA (ds-DNA@Hg^{2+}) with a T-Hg-T coordination motif, and subsequently dissociated into the solution due to its more rigid nature than ss-DNA, leading to the recovery of FAM fluorescence. In the presence of biothiols, including cysteine (Cys), homocysteine (Hcy) and glutathione (GSH), the strong coordination interaction between Hg^{2+} and the mercapto function serves to sequestrate the Hg^{2+} from the ds-DNA@Hg^{2+} duplex. The released ss-DNA, in turn, are re-adsorbed by MOF **1**, leading to the formation of the initial P-DNA@**1** state with fluorescence quenching. As such, P-DNA@**1** detects Hg^{2+} and biothiols Cys/Hcy/GSH in sequence with detection limits of (2.3 ± 0.8) nM and (29.6 ± 0.1) nM/(19.8 ± 0.5) nM/(10.2 ± 0.1) nM. The sensing process is efficient and selective with instantaneous response time. The detection mechanism was further validated by circular dichroism (CD), and simulation studies using Molecular Operating Environment (MOE) package.

1. Introduction

Biological thiols (biothiols), including cysteine (Cys), homocysteine (Hcy) and glutathione (GSH), contain a mercapto group and play important roles in a variety of physiological processes [1]. For example, GSH and Cys are often involved in the reversible redox reactions and cellular functions including metabolism and detoxification [2–6]. Abnormal levels of these biothiols in human serum and urine are associated with many diseases [7,8]. Similarly, Hg^{2+} is one of the most impactful heavy-metal pollutants, and its overdose is causative of brain damage [9], kidney failure, various cognition and motion disorders, and etc. [10]. Importantly, Hg^{2+} has a strong binding affinity toward the mercapto group [11], with the potential to disturb the biothiol level in the physiological system. In addition, the biothiol reaction with Hg^{2+} may cause the inactivation of their enzymes [12]. And the activity of many biothiol-containing enzymes, such as aminotransferases [13,14] and dehydrogenases [15,16], when modified, significantly alter their activities [12]. Therefore, it is of great significance to develop rapid, cost-effective, and reliable methods to sequentially monitor the Hg^{2+} and biothiol levels.

Among various detection assays, fluorescence assay has been promising because of its advantages of high sensitivity, high selectivity, less sample consumption and operational convenience [17]. Thus, many fluorescence sensors based on functional materials, such as gold nanoparticles [5,18], silver nanoclusters [19,20], carbon nanomaterials [21,22], silica nanoparticles [23,24], semiconductor quantum dots [25], graphene oxide (GO) [26,27] have been developed. Among them, the hybrid sensors from these materials with the specific native or artificial DNA bases for the detection of metal ions has aroused increasing interests due to their higher specificity [28,29]. Specifically for Hg^{2+}

* Corresponding author.
E-mail address: jxchen@smu.edu.cn (J.-X. Chen).
[1] These authors contributed equally to this work.

https://doi.org/10.1016/j.jinorgbio.2019.04.004
Received 31 December 2018; Received in revised form 4 April 2019; Accepted 7 April 2019
Available online 16 April 2019
0162-0134/

sensing, the formation of a hairpin-like thymine–Hg^{2+}–thymine (T-Hg-T) motif is ideal [30,31], and a number of DNA-conjugated nanoparticles, nanorods or nanoclusters [32–35] are established as fluorescence biosensors using this concept.

Metal–organic frameworks (MOFs) have also emerged as a new class of functional materials for the detection of detect metal ions and/or biothiols. The widely practiced principle of metal ion detection by a MOF is through decoration of functionalities on the MOF pore surface [36,37]. These functionalities include thiol [38], pyridyl [39], benzimidazolyl [40], methionine [41], and melamine [42], which can specifically interact with metal ions, especially for Hg^{2+} due to its larger ionic radius than many other metal ions [43–48]. The interaction between functional group and Hg^{2+} hinders the energy transfer from organic ligands to metals ions in MOFs, thus cause the alternation of luminescence emission of the MOFs [49]. The biothiol detection by MOFs is operated via the similar way by incorporating functional groups such as maleimide [50,51], malonitrile [52], aldehyde [53], silver nanoparticles [54] etc. in the MOFs. In addition, some inherent catalytic properties of MOFs were also used for biothiol detection [55–57].

More recently, Zhang et al. used the UiO-66-NH_2 MOF to construct a MOF/DNA hybrid for the efficient fluorescent sensing of Hg^{2+} with high sensitivity and selectivity [58]. However, MOF-based hybrid sensing systems that than perform multiple tasks associated with Hg^{2+} and bio-related molecules, either synchronously or successively, is still limited [59]. This is primarily to due to the inherent stability of MOFs in aqueous phase, in addition to a variety of other factors, such as the competitive binding of Hg^{2+} to the carboxylate ligands, and the binding of phosphate from the DNA backbone or the simulated body fluid to the metals from the MOF, both serve to decompose the MOF connectivity [60–62].

We report a one-dimensional (1D) MOF of $[Cu(Cdcbp)(H_2O)_2{\cdot}2H_2O]_n$ (**1**, H_3CdcbpBr = 3-carboxyl-(3,5-dicarboxybenzyl)-pyridinium bromide), which can strongly absorb T-rich single-stranded DNA (ss-DNA) probe labeled with carboxyfluorescein (FAM) (the formed MOF-ss DNA hybrid denotes as P-DNA@**1**) through π-stacking, electrostatic interactions and/or hydrogen bonding interactions, and quenches its fluorescence via a photo-induced electron transfer (PET) process [63–68]. The formed P-DNA@**1** sensing platform can be used for Hg^{2+} detection due to the formation of double-stranded DNA (ds-DNA@Hg^{2+}) through the formation of rigid hairpin-like T-Hg-T motif, which was ejected from MOF **1**, leading to fluorescence recovery. Upon subsequent sequestration of Hg^{2+} by biothiols, including cysteine (Cys), homocysteine (Hcy), and glutathione (GSH), the released P-DNAs are re-adsorbed by MOF **1**, leading to fluorescence quenching again, thus further realized the biothiols detection (Scheme 1).

2. Experimental

2.1. General

IR spectra were recorded on a Nicolet MagNa-IR 550 infrared spectrometer. Elemental analyses for C, H, and N were performed on an EA1110 CHNS elemental analyzer. Powder X-ray diffraction (PXRD) spectra were recorded with a Rigaku D/max-2200/PC. The X-ray generated from a sealed Cu tube was monochromated by a graphite crystal and collimated by a 0.5 mm MONOCAP (λ Cu-Kα = 1.54178 Å). The tube voltage and current were 40 kV and 40 mA, respectively. Fluorescence spectra were measured on an LS55 spectrofluorimeter. Circular dichroism was measured on Applied Photophysics Ltd. (UK) Chirascan plus ACD type circular dichroism spectrometer. The P-DNA, ds-DNA@Hg^{2+} and MOF **1** structures were constructed using Molecular Operating Environment (MOE) package [69]. The initial P-DNA@**1** or **1** + ds-DNA@Hg^{2+} structures were first optimized in MOE using MMFF94x force field and then re-optimized in UFF of Gaussian 09 [70], where Gibbs free energy calculations were simplified by calculating single point energies. Finally, Python molecule (PyMOL) [71] was employed for visual analysis of binding modes.

The DNA sequences (P-DNA: 5′-TTCTTTCTTCCCCTTGTTTGTT-FAM-3′) were purchased from Sangon Inc. (Shanghai, China) and were dissolved in 10 mM Hepes buffer (pH 7.4, Hepes = 2-4-(2-hydroxyethyl)-1-piperazinyl ethane sulfonic acid) and stored at 4 °C for use. The other reagents and solvents were obtained from commercial sources and used without further purification.

2.2. Synthesis of $[Cu(Cdcbp)(H_2O)_2{\cdot}2H_2O]_n$ (1)

Powder of H_3CdcbpBr (38.1 mg, 0.1 mmol) was suspended in H_2O (20 mL) and the pH adjusted to 7.0 with 0.1 M NaOH to give a clear solution, a solution of $CuSO_4{\cdot}5H_2O$ (24.9 mg, 0.1 mmol) in H_2O (20 mL) was subsequently introduced. The resulting mixture was stirred for 15 min to give a clear light-blue solution. After filtration, the filtrate was allowed to stand at ambient temperature for about one week to produce crystals of MOF **1**, which were collected by filtration, washed with ether, and dried under vacuum. Yield: 40.0 mg (92%). Anal. Calcd. for $C_{15}H_{17}NO_{10}Cu{\cdot}2H_2O$: C 38.26, H 4.50, N 2.97. Found: C 38.16, H 4.31, N, 2.86. IR (KBr disc, cm^{-1}) ν 3418 (s), 3036 (s), 1551 (s), 1437 (s), 1369 (s), 1213 (m), 1156 (m), 1019 (w), 768 (s), 713 (s), 642 (m), 540 (m), 486 (m), 441 (m).

3. Results and discussion

3.1. Characterization of MOF 1

MOF **1** is moisture and water stable with the powder X-ray diffraction (PXRD) pattern of the as-synthesized sample, that immersed in H_2O or Hepes buffer, in good agreement with that of the simulated, indicating its bulky phase purity and water stability (Fig. 1a). MOF **1** crystallizes in the triclinic space group *P*–1 and each asymmetric unit contains one $[Cu(Cdcbp)(H_2O)_2]$ molecule and two dissociated H_2O molecules. As shown in Fig. 1b, each Cu(II) is coordinated with two carboxylates from two Cdcbp ligands, both in monodentate fashing, and two additional water molecules, thus forming a quadrilateral geometry. Two carboxylate groups of each ligand connect to two $Cu(H_2O)_2$ units to form a 1D chain structure. The third free and uncoordinated carboxylate each carry a negative charge, thus maintaining the overall charge neutrality of MOF **1**. The detailed crystallographic parameters and the selected bond lengths and angles of MOF **1** (CCDC number 1888000) are listed in Tables 1 and 2, respectively.

3.2. Hg^{2+} detection using the P-DNA@1 hybrid

MOF **1** exhibits a 1D structure with cationic Cu(II) center, conjugated tricarboxylate ligand of Cdcbp bearing positively charged pyridinium and uncoordinated carboxylates, allowing a maximum exposure of these functionalities [72,73]. These features are advantageous in forming π-stacking, electrostatic interactions and/or hydrogen bonding with negatively charged P-DNA sequences.

The fluorescence quenching experiments of P-DNA by MOF **1** were performed by keeping the concentrations of P-DNA constant, while gradually increasing the concentrations of MOF **1** at room temperature. Specifically, aliquots of a solution of MOF **1** containing P-DNA (50 nM) in 10 mM Hepes buffer was added to a solution of P-DNA (50 nM) in the same buffer and stirred to form stable P-DNA@**1** system. As shown in Fig. 2a, the fluorescence intensity of P-DNA decreases gradually with the increase of MOF **1** concentration. When the concentration of MOF **1** reaches 4.0 μM, the fluorescence quenching efficiency (Q_E, %) of P-DNA is (88.0 ± 3.3)%, as calculated according to the equation $Q_E = (F_0 - F_M)/F_0 \times 100\%$, wherein F_M and F_0 are the fluorescence intensity at 518 nm in the presence and absence of MOF **1**, respectively.

In order to investigate the detection time for Hg^{2+}, a solution of $HgCl_2$ was added into the solution of P-DNA@**1** with a concentration of

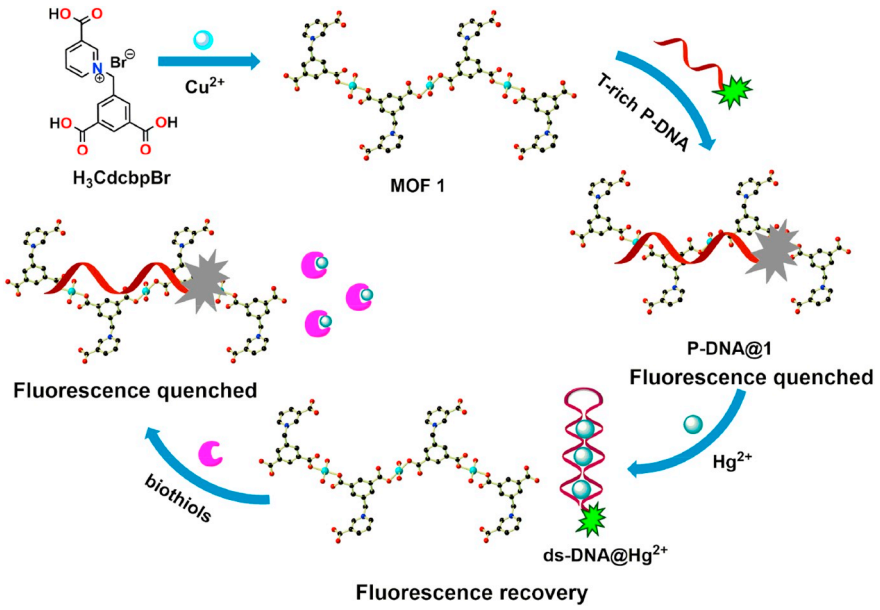

Scheme 1. The proposed Hg^{2+} and biothiols detection mechanism based on the P-DNA@**1** hybrid.

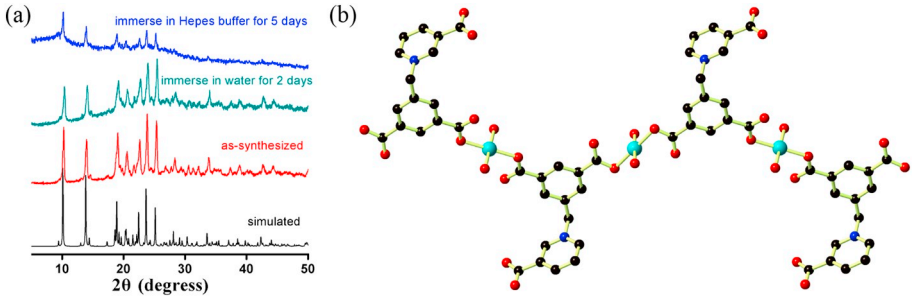

Fig. 1. (a) PXRD patterns of MOF **1** showing agreement among the simulated, as-synthesized, the fresh powder immersed in water for 2 days, and in Hepes buffer for 5 days. (b) The 1D structure of MOF **1**. Color codes: Cu (cyan), O (red), N (blue), C (black).

Table 1
Crystallographic data for MOF **1**.

Molecular formula	$C_{15}H_{17}NO_{10}Cu$		
Crystal system	Triclinic	D_{calc} (g cm^{-3})	1.677
Formula weight	434.84	λ (Mo Kα) (Å)	0.71073
Space group	*P*–1	μ (cm^{-1})	1.326
a (Å)	8.7858(18)	Total reflections	8829
b (Å)	10.289(2)	Unique reflections	3903
c (Å)	10.517(2)	No. observations	3402
α (°)	65.69(3)	No. parameters	247
β (°)	83.62(3)	R^a	0.0404
γ (°)	87.48(3)	wR^b	0.1028
V (Å^3)	861.0(3)	GOF^c	1.054
Z	2	$\Delta\rho_{max}$ (e Å^{-3})	0.800
T/K	293(2)	$\Delta\rho_{min}$ (e Å^{-3})	−0.523

[a] $R_1 = \Sigma||F_o|-|F_c||/\Sigma|F_o|$.
[b] $wR_2 = \{\Sigma[w(F_o^2-F_c^2)^2]/\Sigma[w(F_o^2)^2]\}^{1/2}$.
[c] GOF = $\{\Sigma[w(F_o^2-F_c^2)^2]/(n-p)\}^{1/2}$, where *n* is the number of reflections and *p* is total number of parameters refined.

Table 2
Selected bond lengths (Å) and angles (°) for MOF **1**.

Bond lengths (Å)			
Cu(1)-O(5)	1.9485(18)	Cu(1)-O(5)#1	1.9485(18)
Cu(1)-O(1W)#1	1.943(2)	Cu(1)-O(1W)	1.943(2)
Cu(2)-O(2W)#2	1.943(2)	Cu(2)-O(2W)	1.943(2)
Cu(2)-O(3)	1.9588(18)	Cu(2)-O(3)#2	1.9588(18)

Bond angles (°)			
O(5)-Cu(1)-O(5)#1	180.00(11)	O(5)-Cu(1)-O(1W)#1	89.95(9)
O(5)#1-Cu(1)-O(1W)#1	90.05(9)	O(5)-Cu(1)-O(1W)	90.05(9)
O(5)#1-Cu(1)-O(1W)	89.95(9)	O(1W)#1-Cu(1)-O(1W)	180.00(12)
O(2W)#2-Cu(2)-O(2W)	180.000(1)	O(2W)#2-Cu(2)-O(3)	89.42(9)
O(2W)-Cu(2)-O(3)	90.58(9)	O(2W)#2-Cu(2)-O(3)#2	90.58(9)
O(2W)-Cu(2)-O(3)#2	89.42(9)	O(3)-Cu(2)-O(3)#2	180.00(8)
Cu(1)-O(1W)-H(1W1)	120.5	Cu(1)-O(1W)-H(1W2)	125.0
Cu(2)-O(2W)-H(2W1)	104.0	Cu(2)-O(2W)-H(2W2)	116.8

Symmetry transformations used to generate equivalent atoms:
#1: $-x+1, -y, -z$; #2: $-x+1, -y+2, -z-1$.

0.05 μM and the fluorescence intensity recorded at different time intervals (Fig. 2b). When the time reached 2 min, the fluorescence was completely recovered. The short detection time may due to the 1D chain structure of MOF **1**. Comparing to the 2D and 3D MOFs, MOF **1** with 1D chain structure shows small steric hindrance, and Hg^{2+} can readily induce P-DNA from MOF **1** to form ds-DNA@Hg^{2+} through T-Hg-T base pairs to detach from MOF **1**.

Based on the previous experiment, the fluorescence recovery experiments (R_E, %) were conducted by adding Hg^{2+} of varying concentrations to the P-DNA@**1** sensing platform and maintained for 2 min to give a **1** + ds-DNA@Hg^{2+} mixture. As shown in Fig. 2c, with the increase of Hg^{2+} concentration, the fluorescence intensity of P-DNA rapidly increased. When the Hg^{2+} concentration reaches 0.55 μM, the fluorescence recovery of P-DNA was completed with R_E value being

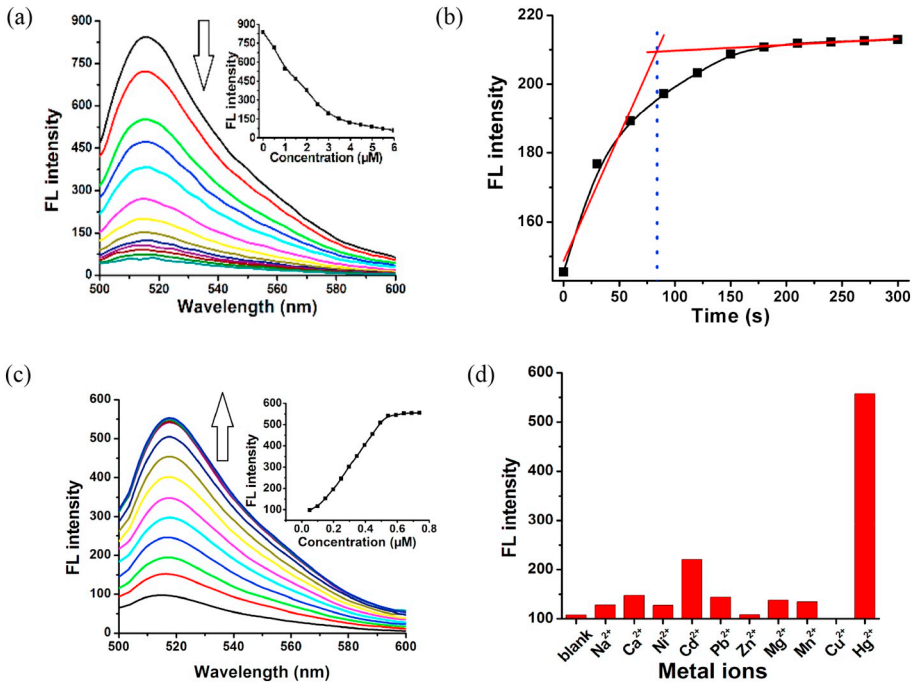

Fig. 2. (a) The fluorescence quenching of the P-DNA (50 nM) incubated with MOF **1** of varying concentrations at room temperature (λ_{ex} = 480 nm, λ_{em} = 518 nm). Inset: plot of fluorescence intensity versus the concentration of MOF **1**. (b) The fluorescence intensity of the P-DNA@**1** (50 nM/4.0 μM) at a function of time for the Hg^{2+} (0.05 μM) detection. (c) The fluorescence spectra of the P-DNA@**1** sensing system (P-DNA@**1**, 50 nM/4.0 μM) incubated with different concentrations of Hg^{2+} in Hepes buffer (pH = 7.4, 10 mM). Inset: plot of the fluorescence intensity versus the concentrations of Hg^{2+}. (d) The selectivity of P-DNA@**1** sensing system toward Hg^{2+} and the other metal ions (Hg^{2+}, 0.6 μM; the other metal ions, 6 μM).

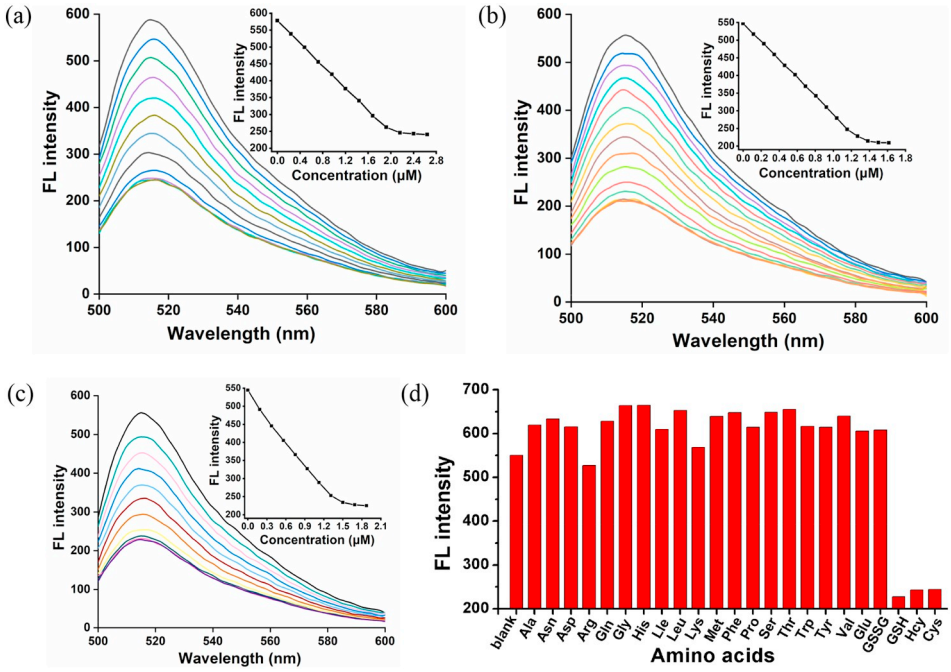

Fig. 3. The fluorescence intensity of the **1** + ds-DNA@Hg^{2+} (4.0 μM/50 nM/0.55 μM/) versus biothiols at different concentrations: Cys (a), GSH (b), and Hcy (c) in Hepes buffer (pH = 7.4, 10 mM) at room temperature. Inset: the fluorescence intensity as a function of concentration of Cys (a), GSH (b), and Hcy (c). (d) The selectivity of the **1** + ds-DNA@Hg^{2+} system toward biothiols and the other amino acids (biothiols, 2.0 μM; the other amino acids, 20.0 μM).

(4.5 ± 0.2), as calculated using the formula $R_E = (F_T - F_M)/F_M$, wherein F_T and F_M are the fluorescence intensities at 518 nm in the presence and the absence of Hg^{2+}, respectively. There is a good linear relationship between the fluorescence intensity and Hg^{2+} concentration from 0.10 to 0.55 μM. According to the $3\delta_b$/slope (δ_b = standard deviation of five blank measurements), the limit of detection (LOD) is calculated to be (2.3 ± 0.8) nM with R^2 = 0.9980 and δ_b = 0.7679, which is lower than the Environmental Protection Agency (EPA) limit of acceptable Hg^{2+} concentration in drinkable water (10 nM) and the toxicity level of Hg^{2+} in drinking water (30 nM) defined by the World Health Organization (WHO) [22,74].

In order to verify whether the P-DNA@**1** sensing platform is selective toward Hg^{2+}, we investigated the fluorescence response of P-DNA@**1** sensing platform to other metal ions, including Na^+, Ca^{2+}, Ni^{2+}, Cd^{2+}, Pb^{2+}, Zn^{2+}, Mg^{2+}, Mn^{2+}, Cu^{2+}, whose concentrations are 10-fold higher than Hg^{2+} using the above method. As shown in Fig. 2d, the fluorescence intensity increased markedly in the presence of Hg^{2+}, while with other metal ions, only very limited changes of the fluorescence intensity are observed, indicating that the P-DNA@**1** sensing platform is capable of specifically recognizing Hg^{2+}.

3.3. Biothiols detection using *1* + *ds-DNA@Hg^{2+}* system

Upon addition of different concentrations of biothiols to the above formed **1** + ds-DNA@Hg^{2+} system, the fluorescence intensity decreased until saturation was observed with the concentration of 2.2 μM for Cys (Fig. 3a), 1.4 μM for GSH (Fig. 3b), 1.8 μM for Hcy (Fig. 3c). The Q_E values are (58.3 ± 1.5)%, (61.6 ± 1.4)% and (58.7 ± 0.4)% for

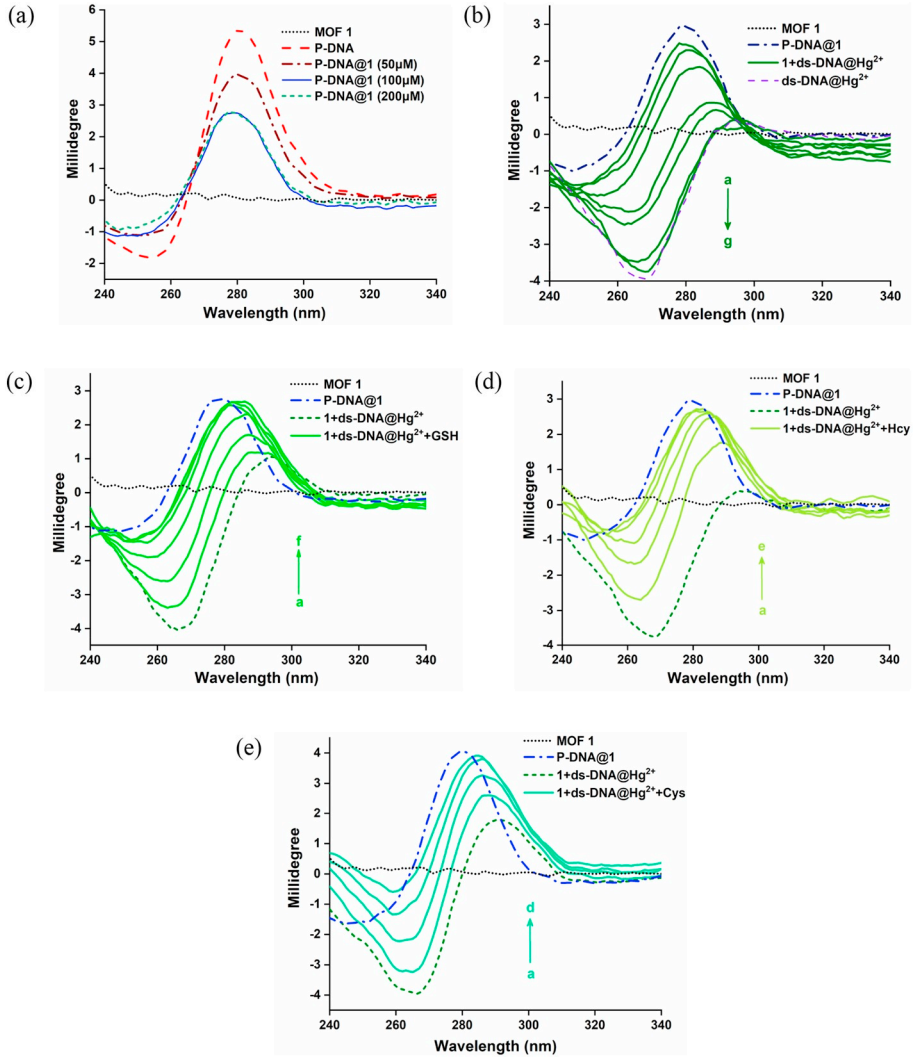

Fig. 4. (a) The CD spectra of P-DNA (10 μM) with different concentrations of MOF **1** (0, 50, 100, 200 μM), (b) the CD spectra of P-DNA@**1** (10 μM/200 μM) with different concentrations of Hg^{2+} (10, 20, 40, 60, 80, 100, 120 μM, a–g) and ds-DNA@Hg^{2+} (10 μM/120 μM), (c) the CD spectra of **1** + ds-DNA@Hg^{2+} (200 μM/10 μM/120 μM) with different concentrations of GSH (30, 60, 90, 120, 150, 180 μM, a–f), as well as (d) Hcy (30, 60, 90, 120, 150 μM, a–e), and (e) Cys (30, 60, 90, 120 μM, a–d).

Cys, GSH and Hcy, respectively. With the good linear relationship between the concentration of biothiols and the fluorescence intensity (from 0 to 1.92 μM with $R^2 = 0.9996$ and $\delta_b = 1.6370$ for Cys, from 0 to 1.27 μM with $R^2 = 0.9999$ and $\delta_b = 0.8674$ for GSH, and from 0 to 1.31 μM with $R^2 = 0.9965$ and $\delta_b = 1.4438$ for Hcy). The LOD are accordingly (29.6 ± 0.1) nM, (10.2 ± 0.1) nM, and (19.8 ± 0.5) nM for Cys, GSH and Hcy.

In order to verify the specificity of the **1** + ds-DNA@Hg^{2+} sensing platform toward biothiols, we further used other amino acids, namely, Ala, Asn, Asp, Arg, Gln, Gly, His, Lle, Leu, Lys, Met, Phe, Pro, Ser, Thr, Trp, Val, Glu, and GSSG, without thiol group as a control. The concentrations of other amino acids are also 10-fold higher than biothiols. It can be concluded from Fig. 3d that the fluorescence exhibits an obvious decay only with the addition of biothiols, suggesting that the **1** + ds-DNA@Hg^{2+} sensing platform can detect biothiols selectively.

To further validate the alternate formation of P-DNA and ds-DNA@Hg^{2+}, we performed a circular dichroism (CD) test during the detection process. At a concentration of 10 μM, the P-DNA has a strong positive peak at 280 nm, while MOF **1** has no CD signal. When increased concentration of MOF **1** was added into the P-DNA solution, the peak intensity gradually decreases, indicating that P-DNA is adsorbed by MOF **1** to form P-DNA@**1**. MOF **1** with highest concentration of 200 μM partially adsorbed P-DNA (10 μM), resulting in partial disappearance of its CD peak (Fig. 4a).

When increased concentration of Hg^{2+} was added to the system of P-DNA@**1**, a new negative peak appeared with slight red shift, coinciding with the peak position of ds-DNA@Hg^{2+} (Fig. 4b). With the ultimate introduction of biothiols, the negative peak of ds-DNA@Hg^{2+} disappeared and the positive peak of P-DNA re-appeared, indicating that biothiols captures Hg^{2+} from the ds-DNA@Hg^{2+} and release P-DNA (Fig. 4c–e).

3.4. Simulation studies of the sensing mechanism

In order to elucidate the detection mechanism, the binding free energy difference ($\Delta\Delta G$) between reactions of MOF **1** with P-DNA ($\Delta G_{P\text{-}DNA@MOF}$) or with ds-DNA@$Hg^{2+}$ ($\Delta G_{MOF+ds\text{-}DNA@Hg^{2+}}$) is calculated. When $\Delta\Delta G < 0$ ($\Delta\Delta G = \Delta G_{P\text{-}DNA@MOF} - \Delta G_{MOF+ds\text{-}DNA@Hg^{2+}}$), meaning that $\Delta G_{P\text{-}DNA@MOF} < \Delta G_{MOF+ds\text{-}DNA@Hg^{2+}}$ and the binding of P-DNA to MOF **1** is stronger than that of ds-DNA@Hg^{2+}, and vice versa. The result showed that $\Delta\Delta G = -28.22$ kcal/mol < 0, suggesting that P-DNA bounds to MOF **1** more tightly than that of ds-DNA@Hg^{2+}, in accordance with the experimental observation.

The electrostatic surface showed that the surface of MOF **1** was

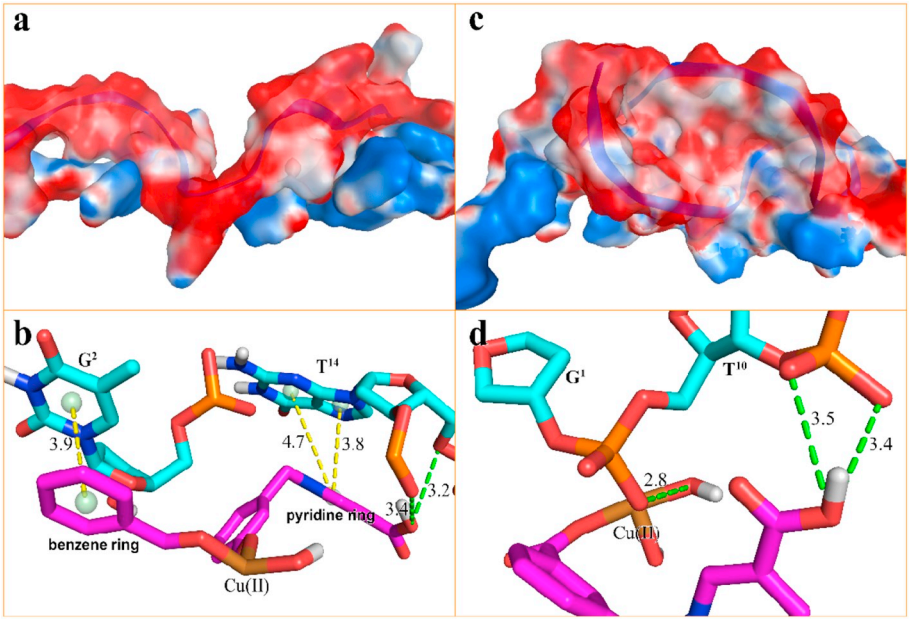

Fig. 5. The interactions between MOF **1** and P-DNA and ds-DNA@Hg^{2+}: (a) and (c) showed the charge distributions where red area represented negative charges, blue positive, and white neutral; (b) and (d) showed the partial local binding modes where MOF **1** was displayed by magenta sticks, while P-DNA or ds-DNA@Hg^{2+} by cyan sticks. Charge centers and aromatic ring centers were denoted by pale green spheres, π-π stacking interactions by yellow dashes, and hydrogen bonding by green dashes.

largely positive and P-DNA was covered by a negative and neutral surface with the scattered positive area, which led to good electronic complement between MOF **1** and P-DNA. Single chain P-DNA exhibits a higher contact area with MOF **1** due to its structural flexibility (Fig. 5a), while double chain ds-DNA@Hg^{2+} only has a small interface (Fig. 5c). MOF **1** bound to P-DNA mainly through ten π-π stacking between the aromatic rings in MOF **1** and heterocycle in P-DNA with the ring centroid distances in the range of 3.8–4.7 Å. This is in addition to six hydrogen bonding between the heterocycle in P-DNA and the carboxylate groups in MOF **1**, with the donor-acceptor distances in the range of 3.2–3.4 Å. In sharp contrast, there are only six hydrogen bonding between oxygen atoms of the phosphate group in ds-DNA@Hg^{2+} and H_2O or carboxylate groups in MOF **1**, with donor-acceptor distances in the range of 2.8–3.5 Å. The partial local binding modes between MOF **1** and P-DNA or ds-DNA@Hg^{2+} was displayed in Fig. 5b and d.

4. Conclusion

In summary, a 1D water-stable Cu(II)–zwitterionic carboxylate MOF **1** has been synthesized and characterized. MOF **1** was subsequently used in the sensitive and specific detection of Hg^{2+} and biothiols in a sequential manner. Such sensing sequence is first enabled by the formation of hairpin-like ds-DNA@Hg^{2+} featuring the T-Hg-T motif (for the sensing of Hg^{2+}, fluorescence on). The established **1** + ds-DNA@Hg^{2+}, in turn, functions as a sensor for Cys, Hcy and GSH, driven by the stronger coordination of mercapto with Hg^{2+} that serves to sequestrate Hg^{2+}, accompanied by the unfolding of ds-DNA into ss-DNA to reach the initial P-DNA@**1** state (fluorescence off). The detection is highly efficient, featuring Hg^{2+} and Cys/Hcy/GSH in sequence with detection limits of (2.3 ± 0.8) nM and (29.6 ± 0.1)/(19.8 ± 0.5)/(10.2 ± 0.1) nM. Our future work involves the development of MOF systems for the synergistic sensing of biologically relevant metal ions and organic species, such as Fe^{3+}/GSH, Fe^{3+}/ascorbic acid, using the simple redox reaction.

Acknowledgments

We are grateful for the financial support from the National Natural Science Foundation of China (21874064), the Natural Science Foundation from Department of Science and Technology of Guangdong Province (2018A030313456) and Southern Medical University. We also thank Dr. Ziying Zhang from Guangzhou Yinfo Information Technology Co., Ltd. for doing the molecular simulation studies.

Appendix A. Supplementary data

Supplementary data to this article can be found online at https://doi.org/10.1016/j.jinorgbio.2019.04.004.

References

[1] S. Zhang, C.N. Ong, H.M. Shen, Critical roles of intracellular thiols and calcium in parthenolide-induced apoptosis in human colorectal cancer cells, Cancer Lett. 208 (2004) 143–153.
[2] S.Y. Liu, F.P. Shi, L. Chen, X.G. Su, Tyrosine-functionalized $CuInS_2$ quantum dots as a fluorescence probe for the determination of biothiols, histidine and threonine, Analyst 138 (2013) 5819–5825.
[3] S. Chen, J.N. Tian, Y.X. Jiang, Y.C. Zhao, J.N. Zhang, S.L. Zhao, A one-step selective fluorescence turn-on detection of cysteine and homocysteine based on a facile CdTe/CdS quantum dots-phenanthroline system, Anal. Chim. Acta 787 (2013) 181–188.
[4] S.K. Sun, H.F. Wang, X.P. Yan, A sensitive and selective resonance light scattering bioassay for homocysteine in biological fluids based on target-involved assembly of polyethyleneimine-capped Ag-nanoclusters, Chem. Commun. 47 (2011) 3817–3819.
[5] M. Zhang, M.X. Yu, F.Y. Li, M.W. Zhu, M.Y. Li, Y.H. Gao, L. Li, Z.Q. Liu, J.P. Zhang, D.Q. Zhang, T. Yi, C.H. Huang, A highly selective fluorescence turn-on sensor for cysteine/homocysteine and its application in bioimaging, J. Am. Chem. Soc. 129 (2007) 10322–10323.
[6] Z.Y. Yao, H. Bai, C. Li, G.Q. Shi, Colorimetric and fluorescent dual probe based on a polythiophene derivative for the detection of cysteine and homocysteine, Chem. Commun. 47 (2011) 7431–7433.
[7] T.P. Dalton, H.G. Shertzer, A. Puga, Regulation of gene expression by reactive oxygen, Annu. Rev. Pharmacol. Toxicol. 39 (1999) 67–101.
[8] D.M. Townsend, K.D. Tew, H. Tapiero, The importance of glutathione in human disease, Biomed. Pharmacother. 57 (2003) 145–155.
[9] D.J. Yang, S. Shi, T.M. Yao, L.N. Ji, Cooperative folding of tau peptide by coordination of group IIB metal cations during heparin-induced aggregation, Biometals 25 (2012) 361–372.
[10] P.B. Tchounwou, W.K. Ayensu, N. Ninashvili, D. Sutton, Environmental exposure to mercury and its toxicopathologic implications for public health, Environ. Toxicol. 18 (2003) 149–175.
[11] B.J. Fuhr, D.L. Rabenstein, Nuclear magnetic resonance studies of the solution chemistry of metal complexes. IX. The binding of cadmium, zinc, lead, and mercury by glutathione, J. Am. Chem. Soc. 95 (1973) 6944–6950.
[12] C.C. Bridges, B.F. Krasnikov, L. Joshee, J.T. Pinto, A. Hallen, J. Li, R.K. Zalups, A.J. Cooper, New insights into the metabolism of organomercury compounds: mercury-containing cysteine S-conjugates are substrates of human glutamine transaminase K and potent inactivators of cystathionine gamma-lyase, Arch. Biochem. Biophys. 517 (2012) 20–29.
[13] W. Birchmeier, K.J. Wilson, P. Christen, Cytoplasmic aspartate aminotransferase: syncatalytic sulfhydryl group modification, J. Biol. Chem. 248 (1973) 1751–1759.
[14] T.G. Kalogerakos, N.G. Oikonomakos, C.G. Dimitropoulos, I.A. Karni-katsadima, A.E. Evangelopoulos, Interaction of aspartate aminotransferase with

mercurochrome. Relationship of an exposed thiol group of the enzyme to the active centre, Biochem. J. 167 (1977) 53–63.
[15] G.G. Chang, R.Y. Hsu, Mechanism of pigeon liver malic enzyme: kinetics, specificity, and half-site stoichiometry of the alkylation of a cysteinyl residue by the substrate-inhibitor bromopyruvate, Biochemistry 16 (1977) 311–320.
[16] K. Pamp, T. Bramey, M. Kirsch, H. De Groot, F. Petrat, NAD(H) enhances the Cu(II)-mediated inactivation of lactate dehydrogenase by increasing the accessibility of sulfhydryl groups, Free Radic. Res. 39 (2005) 31–40.
[17] C.C. Wang, D. Zhang, X.Y. Huang, P.G. Ding, Z.J. Wang, Y.F. Zhao, Y. Ye, A ratiometric fluorescent chemosensor for Hg^{2+} based on FRET and its application in living cells, Sensors Actuators B Chem. 198 (2014) 33–40.
[18] B. Paramanik, S. Bhattacharyya, A. Patra, Detection of Hg^{2+} and F^- ions by using fluorescence switching of quantum dots in an Au-cluster-CdTe QD nanocomposite, Chem. Eur. J. 19 (2013) 5980–5987.
[19] J. Duan, H. Yin, R. Wei, W. Wang, Facile colorimetric detection of Hg^{2+} based on anti-aggregation of silver nanoparticles, Biosens. Bioelectron. 57 (2014) 139–142.
[20] L. Deng, Z. Zhou, J. Li, T. Li, S. Dong, Fluorescent silver nanoclusters in hybridized DNA duplexes for the turn-on detection of Hg^{2+} ions, Chem. Commun. 47 (2011) 11065–11067.
[21] H.L. Li, J.F. Zhai, X.P. Sun, Nano-C_{60} as a novel, effective fluorescent sensing platform for mercury(II) ion detection at critical sensitivity and selectivity, Nanoscale 3 (2011) 2155–2157.
[22] L.B. Zhang, L. Tao, B.L. Li, L. Jing, E.K. Wang, Carbon nanotube-DNA hybrid fluorescent sensor for sensitive and selective detection of mercury(II) ion, Chem. Commun. 46 (2010) 1476–1478.
[23] D.G. He, X.X. He, K.M. Wang, M.A. Chen, Y.X. Zhao, Z. Zou, Intracellular acid-triggered drug delivery system using mesoporous silica nanoparticles capped with T-Hg^{2+}-T base pairs mediated duplex DNA, J. Mater. Chem. B 1 (2013) 1552–1560.
[24] Z. Zhang, D. Balogh, F. Wang, I. Willner, Smart mesoporous SiO_2 nanoparticles for the DNAzyme-induced multiplexed release of substrates, J. Am. Chem. Soc. 135 (2013) 1934–1940.
[25] R. Freeman, X.Q. Liu, I. Willner, Chemiluminescent and chemiluminescence resonance energy transfer (CRET) detection of DNA, metal ions, and aptamer-substrate complexes using hemin/G-quadruplexes and CdSe/ZnS quantum dots, J. Am. Chem. Soc. 133 (2011) 11597–11604.
[26] J.H. Huang, X. Gao, J.J. Jia, J.K. Kim, Z.G. Li, Graphene oxide-based amplified fluorescent biosensor for Hg^{2+} betection through hybridization chain reactions, Anal. Chem. 86 (2014) 3209–3215.
[27] S.J. He, B. Song, D. Li, C.F. Zhu, W.P. Qi, Y.Q. Wen, L.H. Wang, S.P. Song, H.P. Fang, C.H. Fan, A graphene nanoprobe for rapid, sensitive, and multicolor fluorescent DNA analysis, Adv. Funct. Mater. 20 (2010) 453–459.
[28] A. Porchetta, A. Vallee-Belisle, K.W. Plaxco, F. Ricci, Allosterically tunable, DNA-based switches triggered by heavy metals, J. Am. Chem. Soc. 135 (2013) 13238–13241.
[29] J.M. Thomas, H.Z. Yu, D. Sen, A mechano-electronic DNA switch, J. Am. Chem. Soc. 134 (2012) 13738–13748.
[30] A. Ono, H. Togashi, Highly selective oligonucleotide-based sensor for mercury(II) in aqueous solutions, Angew. Chem. Int. Ed. Engl. 43 (2004) 4300–4302.
[31] Y. Miyake, H. Togashi, M. Tashiro, H. Yamaguchi, S. Oda, M. Kudo, Y. Tanaka, Y. Kondo, R. Sawa, T. Fujimoto, T. Machinami, A. Ono, $Mercury^{II}$-mediated formation of thymine-Hg^{II}-thymine base pairs in DNA duplexes, J. Am. Chem. Soc. 128 (2006) 2172–2173.
[32] J.S. Lee, M.S. Han, C.A. Mirkin, Colorimetric detection of mercuric ion (Hg^{2+}) in aqueous media using DNA-functionalized gold nanoparticles, Angew. Chem. Int. Ed. 46 (2007) 4093–4096.
[33] W.W. Guo, J.P. Yuan, E.K. Wang, Oligonucleotide-stabilized Ag nanoclusters as novel fluorescence probes for the highly selective and sensitive detection of the Hg^{2+} ion, Chem. Commun. (2009) 3395–3397.
[34] Z.Z. Huang, F. Pu, Y.H. Lin, J.S. Ren, X.G. Qu, Modulating DNA-templated silver nanoclusters for fluorescence turn-on detection of thiol compounds, Chem. Commun. 47 (2011) 3487–3489.
[35] Y.Y. Zhu, L.G. Xu, W. Ma, Z. Xu, H. Kuang, L.B. Wang, C.L. Xu, A one-step homogeneous plasmonic circular dichroism detection of aqueous mercury ions using nucleic acid functionalized gold nanorods, Chem. Commun. 48 (2012) 11889–11891.
[36] T.Y. Gu, M. Dai, D.J. Young, Z.G. Ren, J.P. Lang, Luminescent Zn(II) coordination polymers for highly selective sensing of Cr(III) and Cr(VI) in water, Inorg. Chem. 56 (2017) 4669–4679.
[37] F.L. Hu, Y.X. Shi, H.H. Chen, J.P. Lang, A Zn(II) coordination polymer and its photocycloaddition product: syntheses, structures, selective luminescence sensing of iron(III) ions and selective absorption of dyes, Dalton Trans. 44 (2015) 18795–18803.
[38] K.K. Yee, N. Reimer, J. Liu, S.Y. Cheng, S.M. Yiu, J. Weber, N. Stock, Z. Xu, Effective mercury sorption by thiol-laced metal-organic frameworks: in strong acid and the vapor phase, J. Am. Chem. Soc. 135 (2013) 7795–7798.
[39] J. Yang, Z. Wang, Y.S. Li, Q.X. Zhuang, W.R. Zhao, J.L. Gu, Porphyrinic MOFs for reversible fluorescent and colorimetric sensing of mercury(II) ions in aqueous phase, RSC Adv. 6 (2016) 69807–69814.
[40] F. Xu, L. Kou, J. Jia, X.D. Hou, Z. Long, S.L. Wang, Metal-organic frameworks of zeolitic imidazolate framework-7 and zeolitic imidazolate framework-60 for fast mercury and methylmercury speciation analysis, Anal. Chim. Acta 804 (2013) 240–245.
[41] M. Mon, F. Lloret, J. Ferrando-Soria, C. Marti-Gastaldo, D. Armentano, E. Pardo, Selective and efficient removal of mercury from aqueous media with the highly flexible arms of a bioMOF, Angew. Chem. Int. Ed. 55 (2016) 11167–11172.
[42] T. Xia, T. Song, G. Zhang, Y. Cui, Y. Yang, Z. Wang, G. Qian, A terbium metal-organic framework for highly selective and sensitive luminescence sensing of Hg^{2+} ions in aqueous solution, Chem. Eur. J. 22 (2016) 18429–18434.
[43] Y.P. Zhu, T.Y. Ma, T.Z. Ren, Z.Y. Yuan, Mesoporous cerium phosphonate nanostructured hybrid spheres as label-free Hg^{2+} fluorescent probes, ACS Appl. Mater. Interfaces 6 (2014) 16344–16351.
[44] M.M. Liu, G. Li, Z.H. Cheng, A novel dual-functional fluorescent chemosensor for the selective detection of 2,4,6-trinitrotoluene and Hg^{2+}, New J. Chem. 39 (2015) 8484–8491.
[45] S.S.J. Xavier, G. Siva, J. Annaraj, A.R. Kim, D.J. Yoo, G.G. Kumar, Sensitive and selective turn-off-on fluorescence detection of Hg^{2+} and cysteine using nitrogen doped carbon nanodots derived from citron and urine, Sensors Actuators B Chem. 259 (2018) 1133–1143.
[46] W.X. Li, H.X. Li, H.Y. Li, M.M. Chen, Y.X. Shi, J.P. Lang, 1,4-Bis(2-(pyridin-4-yl) vinyl)naphthalene and its zinc(II) coordination polymers: synthesis, structural characterization, and selective luminescent sensing of mercury(II) ion, Cryst. Growth Des. 17 (2017) 3948–3959.
[47] W.J. Gong, Z.G. Ren, H.X. Li, J.G. Zhang, J.P. Lang, Cadmium(II) coordination polymers of 4-pyr-poly-2-ene and carboxylates: construction, structure, and photochemical double [2+2] cycloaddition and luminescent sensing of nitroaromatics and mercury(II) ions, Cryst. Growth Des. 17 (2017) 870–881.
[48] W.J. Gong, R. Yao, H.X. Li, Z.G. Ren, J.G. Zhang, J.P. Lang, Luminescent cadmium (II) coordination polymers of 1,2,4,5-tetrakis(4-pyridylvinyl)benzene used as efficient multi-responsive sensors for toxic metal ions in water, Dalton Trans. 46 (2017) 16861–16871.
[49] A. Dorazco-González, M.F. Alamo, C. Godoy-Alcántar, H. Höpfl, A.K. Yatsimirsky, Fluorescent anion sensing by bisquinolinium pyridine-2,6-dicarboxamide receptors in water, RSC Adv. 4 (2013) 455–466.
[50] S.F. Xue, L.F. Lu, Q.X. Wang, S.Q. Zhang, M. Zhang, G.Y. Shi, An integrated logic system for time-resolved fluorescent "turn-on" detection of cysteine and histidine base on terbium (III) coordination polymer-copper (II) ensemble, Talanta 158 (2016) 208–213.
[51] Y.A. Li, C.W. Zhao, N.X. Zhu, Q.K. Liu, G.J. Chen, J.B. Liu, X.D. Zhao, J.P. Ma, S.J. Zhang, Y.B. Dong, Nanoscale UiO-MOF-based luminescent sensors for highly selective detection of cysteine and glutathione and their application in bioimaging, Chem. Commun. 51 (2015) 17672–17675.
[52] H.W. Li, X. Feng, Y.X. Guo, D.D. Chen, R. Li, X.Q. Ren, X. Jiang, Y.P. Dong, B. Wang, A malonitrile-functionalized metal-organic framework for hydrogen sulfide detection and selective amino acid molecular recognition, Sci. Rep. 4 (2014) 4366.
[53] J. Wang, Y. Liu, M. Jiang, Y. Li, L. Xia, P. Wu, Aldehyde-functionalized metal-organic frameworks for selective sensing of homocysteine over Cys, GSH and other natural amino acids, Chem. Commun. 54 (2018) 1004–1007.
[54] X. Kuang, S.J. Ye, X.Y. Li, Y. Ma, C.Y. Zhang, B. Tang, A new type of surface-enhanced Raman scattering sensor for the enantioselective recognition of D/L-cysteine and D/L-asparagine based on a helically arranged Ag NPs@homochiral MOF, Chem. Commun. 52 (2016) 5432–5435.
[55] H. Hosseini, H. Ahmar, A. Dehghani, A. Bagheri, A. Tadjarodi, A.R. Fakhari, A novel electrochemical sensor based on metal-organic framework for electro-catalytic oxidation of L-cysteine, Biosens. Bioelectron. 42 (2013) 426–429.
[56] N. Yang, H. Song, X. Wan, X. Fan, Y. Su, Y. Lv, A metal (Co)-organic framework-based chemiluminescence system for selective detection of L-cysteine, Analyst 140 (2015) 2656–2663.
[57] X. Yuhao, C. Siheng, Y. Fanggui, S. Lingjing, Z. Cong, S. Shufen, Z. Shulin, Synthesis of a mixed valence state Ce-MOF as an oxidase mimetic for the colorimetric detection of biothiols, Chem. Commun. 51 (2015) 4635–4638.
[58] L.L. Wu, Z. Wang, S.N. Zhao, X. Meng, X.Z. Song, J. Feng, S.Y. Song, H.J. Zhang, A metal-organic framework/DNA hybrid system as a novel fluorescent biosensor for mercury(II) ion detection, Chem. Eur. J. 22 (2016) 477–480.
[59] P.P. Hu, N. Liu, K.Y. Wu, L.Y. Zhai, B.P. Xie, B. Sun, W.J. Duan, W.H. Zhang, J.X. Chen, Successive and specific detection of Hg^{2+} and I^- by a DNA@MOF biosensor: experimental and simulation studies, Inorg. Chem. 57 (2018) 8382–8389.
[60] J.X. Chen, W.H. Zhang, X.Y. Tang, Z.G. Ren, Y. Zhang, J.P. Lang, Assembly of a new family of mercury(II) zwitterionic thiolate complexes from a preformed compound $[Hg(Tab)_2](PF_6)_2$ [Tab = 4-(trimethylammonio)benzenethiolate], Inorg. Chem. 45 (2006) 2568–2580.
[61] X.Y. Tang, A.X. Zheng, H. Shang, R.X. Yuan, H.X. Li, Z.G. Ren, J.P. Lang, Binding of a coordinatively unsaturated mercury(II) thiolate compound by carboxylate anions, Inorg. Chem. 50 (2011) 503–516.
[62] X.Y. Tang, H.X. Li, J.X. Chen, Z.G. Ren, J.P. Lang, Synthetic and structural chemistry of groups 11 and 12 metal complexes of the zwitterionic ammonium thiolate ligands, Coord. Chem. Rev. 252 (2008) 2026–2049.
[63] S.P. Yang, S.R. Chen, S.W. Liu, X.Y. Tang, L. Qin, G.H. Qiu, J.X. Chen, W.H. Chen, Platforms formed from a three-dimensional Cu-based zwitterionic metal-organic framework and probe ss-DNA: selective fluorescent biosensors for human immunodeficiency virus 1 ds-DNA and Sudan virus RNA sequences, Anal. Chem. 87 (2015) 12206–12214.
[64] L. Qin, L.X. Lin, Z.P. Fang, S.P. Yang, G.H. Qiu, J.X. Chen, W.H. Chen, A water-stable metal-organic framework of a zwitterionic carboxylate with dysprosium: a sensing platform for Ebolavirus RNA sequences, Chem. Commun. 52 (2015) 132–135.
[65] S.P. Yang, W. Zhao, P.P. Hu, K.Y. Wu, Z.H. Jiang, L.P. Bai, M.M. Li, J.X. Chen, Lanthanum-based metal-organic frameworks for specific detection of Sudan virus RNA conservative sequences down to single-base mismatch, Inorg. Chem. 56 (2017) 14880–14887.
[66] G.H. Qiu, Z.H. Weng, P.P. Hu, W.J. Duan, B.P. Xie, B. Sun, X.Y. Tang, J.X. Chen, Synchronous detection of ebolavirus conserved RNA sequences and ebolavirus-encoded miRNA-like fragment based on a zwitterionic copper (II) metal-organic

framework, Talanta 180 (2018) 396–402.
[67] B. Sun, Z. Liang, B.P. Xie, R.T. Li, L.Z. Li, Z.H. Jiang, L.P. Bai, J.X. Chen, Fluorescence sensing platform based on ruthenium(II) complexes as high 3S (sensitivity, specificity, speed) and "on-off-on" sensors for the miR-185 detection, Talanta 179 (2017) 658–667.
[68] B.P. Xie, G.H. Qiu, P.P. Hu, Z. Liang, Y.M. Liang, B. Sun, L.P. Bai, Z.H. Jiang, J.X. Chen, Simultaneous detection of Dengue and Zika virus RNA sequences with a three-dimensional Cu-based zwitterionic metal–organic framework, comparison of single and synchronous fluorescence analysis, Sensors Actuators B Chem. 254 (2018) 1133–1140.
[69] Molecular Operating Environment (MOE), 2014.09, Chemical Computing Group Inc., 1010 Sherbooke St. West, Suite #910, Montreal, QC, Canada, H3A 2R7, 2014.
[70] M.J. Frisch, G.W. Trucks, H.B. Schlegel, G.E. Scuseria, M.A. Robb, J.R. Cheeseman, G. Scalmani, V. Barone, B. Mennucci, G.A. Petersson, H. Nakatsuji, M. Caricato, X. Li, H.P. Hratchian, A.F. Izmaylov, J. Bloino, G. Zheng, J.L. Sonnenberg, M. Hada, M. Ehara, K. Toyota, R. Fukuda, J. Hasegawa, M. Ishida, T. Nakajima, Y. Honda, O. Kitao, H. Nakai, T. Vreven, J.A. Montgomery Jr., J.E. Peralta, F. Ogliaro, M. Bearpark, J.J. Heyd, E. Brothers, K.N. Kudin, V.N. Staroverov, R. Kobayashi, J. Normand, K. Raghavachari, A. Rendell, J.C. Burant, S.S. Iyengar, J. Tomasi, M. Cossi, N. Rega, J.M. Millam, M. Klene, J.E. Knox, J.B. Cross, V. Bakken, C. Adamo, J. Jaramillo, R. Gomperts, R.E. Stratmann, O. Yazyev, A.J. Austin, R. Cammi, C. Pomelli, J.W. Ochterski, R.L. Martin, K. Morokuma, V.G. Zakrzewski, G.A. Voth, P. Salvador, J.J. Dannenberg, S. Dapprich, A.D. Daniels, O. Farkas, J.B. Foresman, J.V. Ortiz, J. Cioslowski, D.J. Fox, Gaussian 09, Revision D.01, Gaussian, Inc., Wallingford CT, 2013.
[71] L.L.C. Schrödinger, The PyMOL Molecular Graphics System, Version 1.8, (2015).
[72] B. Wu, W.H. Zhang, J.P. Lang, Site-selective homo- and hetero-metallic doping of a 1D Zn-based coordination polymer to enhance the dimensionality and photocurrent responses, CrystEngComm 18 (2016) 3048–3054.
[73] B. Wu, W.H. Zhang, Z.G. Ren, J.P. Lang, A 1D anionic coordination polymer showing superior Congo Red sorption and its dye composite exhibiting remarkably enhanced photocurrent response, Chem. Commun. 51 (2015) 14893–14896.
[74] L. Deng, X. Ouyang, J. Jin, C. Ma, Y. Jiang, J. Zheng, J. Li, Y. Li, W. Tan, R. Yang, Exploiting the higher specificity of silver amalgamation: selective detection of mercury(II) by forming Ag/Hg amalgam, Anal. Chem. 85 (2013) 8594–8600.